STRUCTURE PRESERVING FORMULATION OF HIGH **VISCOUS FLUID FLOWS**

Mechanical Engineering
Technical Report ME-TR-9

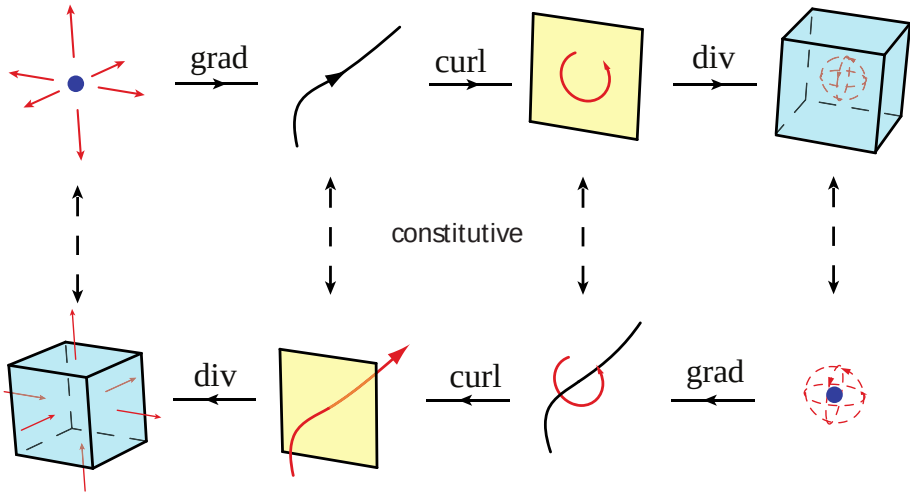

AARHUS
UNIVERSITY
DEPARTMENT OF ENGINEERING

DATA SHEET

Titel: Structure preserving formulation of high viscous fluid flows.
Subtitle: Mechanical Engineering
Series title and no.: Technical Report ME-TR-9

Author: Kennet Olesen
Department of Engineering – Mechanical Engineering, Aarhus University

Internet version: The report is available in electronic format (pdf) at the Department of Engineering website http://www.eng.au.dk.

Publisher: Aarhus University©
URL: http://www.eng.au.dk

Year of publication: 2014 Pages: 31
Editing completed: November 2014

Abstract: This report contains the progress status of the PhD project titled "Structure preserving formulation of high viscous fluid flows". It describes the first ideas to a numerical scheme, which conserves mass and momentum in a discrete sense. It is based on spectral expansion polynomials, and it is thought to be applicable to arbitrary constitutive fluid models.

Keywords: Computer aided engineering, Continuum mechanics, Numerical Modelling, Fluid mechanics, Non-Newtonian fluids, Spectral methods, Structure preserving methods

Referee/Supervisor: Bo Gervang (main supervisor), Henrik Myhre Jensen and Marc Gerritsma

Please cite as: Kennet Olesen, 2014. Structure preserving formulation of high viscous fluid flows. Department of Engineering, Aarhus University. Denmark. 31 pp. - Technical report ME-TR-9

Cover image: Kennet Olesen

ISSN: 2245-4594

STRUCTURE PRESERVING FORMULATION OF HIGH VISCOUS FLUID FLOWS

Kennet Olesen, Aarhus University

Abstract

This report contains the progress status of the PhD project titled “Structure preserving formulation of high viscous fluid flows”. It describes the first ideas to a numerical scheme, which conserves mass and momentum in a discrete sense. It is based on spectral expansion polynomials, and it is thought to be applicable to arbitrary constitutive fluid models.

Contents

Preface

The following report describes the progress of my PhD project and the outcome of the work done in the period 1st of June 2013 to the 7th of November 2014. The report is a part of the PhD program at the Graduate School of Science and Technology at Aarhus University.

This work is addressed to the PhD comity, the supervisors of the present PhD study and the examiner.

A special thanks is given to:

- Bo Gervang, Aarhus University, for guidance throughout the project.
- Henrik Myhre Jensen, Aarhus University, for supervision.
- Marc Gerritsma, TU Delft, for his untiring efforts to teach me the mimetic idea and theory.
- My PhD colleagues Jens Lycke Wind, Per Christian Hyldahl, Alex Møberg, Søren Bøgelund Madsen, Mads Krabbe, Søren Steffenson and Evelien de Olde for daily correspondence and a fun working environment.

I know that the total number of pages exceeds the maximum of 30, but since the additional pages are auxiliary pages like, preface, table of contents, bibliography and glossary, I hope this is acceptable.

Kennet Ryan Olesen

formulation is used. Here the vorticity is inserted in a version of the momentum equations, where these have been merged with the Newtonian constitutive relation, and hence there is not a clear distinction between momentum balance and constitutive relations any more.

The goal of this PhD project is to develop a high order structure preserving formulation of the Stokes equation for an arbitrary incompressible fluid where mass and momentum are preserved to machine precision. The basic Stokes momentum equations are used which contain pressure and viscous stresses, and the constitutive relation are then solved as a separate equation. A clear separation between balance and constitutive equations is hence maintained. The unknowns in the system is the velocity components, the pressure and the viscous stress components, which for a 3D system consist of 6 individual components. Typically, only the velocity components and the pressure are solved for in Newtonian fluid flow, so adding 6 components could seem to be complicating the system unnecessarily. This is though commonly done in the non-Newtonian field of CFD, where the models only have implicit expression for the stresses, and so the new formulation is able to simulate arbitrary constitutive models. The performance of the formulation is to be compared with the high order FEM and the FVM methods on various test cases.

Mimetic methods on non-Newtonian fluids are basically a new topic, so the methods are to be developed from scratch. This means that a lot of theory has to be learned and applied in new ways and trial and error is inevitable. The literature concerning mimetic methods extensively rely on differential geometry. This topic is deliberately avoided in this report, as it is an unknown field to many, and the theory can be often be related to more familiar mathematical terms.

This progress report is structured as follows. First rheology is explained giving examples of fluid behaviour and how it can be modelled. Rheology is a vast area and only the essentials are explained. Next the theory of the high order FEM method is explained giving numerical examples to show the superior convergence. Then the mimetic or structure preserving approach is explained. The report is finalised by a conclusion and a future work section.

2 Rheology

The definition of rheology is that it is the branch of physics concerned with the flow and change of shape of matter. The physical behaviour of a fluid is described by the momentum conservation law:

$$\frac{\partial(\rho \boldsymbol{u})}{\partial t} + \nabla \cdot (\rho \boldsymbol{u}\boldsymbol{u}) = -\nabla \cdot \boldsymbol{\Pi} + \boldsymbol{f}_{ext}, \tag{2.1}$$

the mass conservation law:

$$\frac{\partial \rho}{\partial t} + \nabla \cdot (\rho \boldsymbol{u}) = 0 \tag{2.2}$$

and some constitutive equation, which describes the relation between stresses and deformation. Rheology is the study of such relations. In (2.1) and (2.2) ρ is the density of the fluid, $\boldsymbol{u}$ is the velocity vector, $\boldsymbol{\Pi}$ is the total stress tensor and $\boldsymbol{f}_{ext}$ is a force vector describing the external body forces (e.g. gravity given by $\boldsymbol{f}_{ext} = \rho \boldsymbol{g}$, where $\boldsymbol{g}$ is the gravitational acceleration). Both (2.1) and (2.2) are derived by looking at the momentum and mass balance on an arbitrary volume. The fluxes over the boundaries are equated to the internal contributions. The total stress tensor, $\boldsymbol{\Pi}$, is the momentum flux over the boundaries of the arbitrary volume, and it is divided in two parts:

$$\boldsymbol{\Pi} = p\boldsymbol{I} + \boldsymbol{\tau}. \tag{2.3}$$

The thermodynamic pressure, p, is related to the density and temperature of the fluid through an equation of state, e.g. the ideal gas law. The viscous stress tensor $\boldsymbol{\tau}$ on the other hand is related to the deformation rate of the fluid, and is hence zero, when the fluid is stationary. For non-isothermal flows it is also required to consider the conservation of internal energy and include constitutive relations relating the temperature to the internal energy like the Fourier's law of heat conduction. By assuming that the system is isothermal allows a substantial reduction in complexity. Since the fluid of interest often is quite dense an incompressibility assumption can be introduced without significant errors. This makes the equation of state redundant, as the density now is a constant value. This reduces (2.1) and (2.2) to:

$$\rho \left(\frac{\partial(\boldsymbol{u})}{\partial t} + \boldsymbol{u} \cdot \nabla \boldsymbol{u} \right) = -\nabla \cdot \boldsymbol{\Pi} + \boldsymbol{f}_{ext}, \tag{2.4}$$

and

$$\nabla \cdot \boldsymbol{u} = 0. \tag{2.5}$$

These two equations are common in all incompressible isothermal flows, and the only thing that separates different flows are the boundary conditions, the initial conditions and the viscous stress/strain-rate relation, where the latter can be quite challenging to describe. The viscosity of the fluid of interest can change during the flow and memory effects can be present.

2.1 Newtonian fluids

There are a special class of fluids which have a linear relation between the viscous stress and the deformation rate. These are called Newtonian fluid, because it was Newton, who discovered this relation. These fluids have no memory effect, so they adapt to their container instantaneously.

Water and air are two examples of such fluids and hence many engineering problems can be described using this relation, which is called Newton's law of viscosity:

$$\boldsymbol{\tau} = -2\mu\dot{\boldsymbol{\gamma}}. \tag{2.6}$$

Here $\dot{\boldsymbol{\gamma}}$ is the symmetric part of the strain-rate tensor:

$$\dot{\boldsymbol{\gamma}} = \frac{1}{2}\left(\nabla \boldsymbol{u} + (\nabla \boldsymbol{u})^T\right). \tag{2.7}$$

μ is the viscosity of the fluid and is a constant. This reduces the complexity of the calculation, as (2.6) and (2.7) can be inserted directly into (2.4). Unfortunately the majority of all fluids do not have this simple relation between viscous stress and strain-rate, and explicit expressions for the viscous stress tensor cannot be derived.

2.2 Shear thinning and shear thickening

One of the most commonly seen properties of non-Newtonian fluids are their ability to change viscosity through a flow. Especially shear thinning is observed in many fluid. Ketchup for instance are quite thick and flows slowly in the beginning, but as the deformation rate increases, it becomes thinner and flows more rapidly. On Figure 2.1 a typical example of this behaviour is shown, where the viscosity of different suspensions of polydimethylsiloxanes is plotted as a function of the shear rate. As seen the viscosity is near constant at low shear rates, but as this is increased the viscosity decreases exponentially (it is linear in the logarithmic plot). Sometimes a lower level is also observed, where the viscosity becomes constant again. This can be observed in Figure 2.2, where a 55 % concentration of cornstarch in water suspension is tested. Here the viscosity drops to a lower limit, but then starts to increase rapidly again until an upper limit is reached. This is an example of a shear thickening fluid. There are several models, which replicates the behaviour of shear thinning and shear thickening. Two of the most commonly known are presented. The power law model is able to simulate the exponential decrease/increase of viscosity:

$$\eta\left(\dot{\gamma}\right) = m\dot{\gamma}^{n-1}, \tag{2.8}$$

where n determines the slope of the exponential region in the logarithmic scale, and m shifts the constant along the y-axis. The Carreau-Yasuda model on the other hand are also able to simulate upper and lower limits of the viscosity:

$$\frac{\eta - \eta_\infty}{\eta_0 - \eta_\infty} = \left(1 + (\lambda\dot{\gamma})^a\right)^{\frac{n-1}{a}}. \tag{2.9}$$

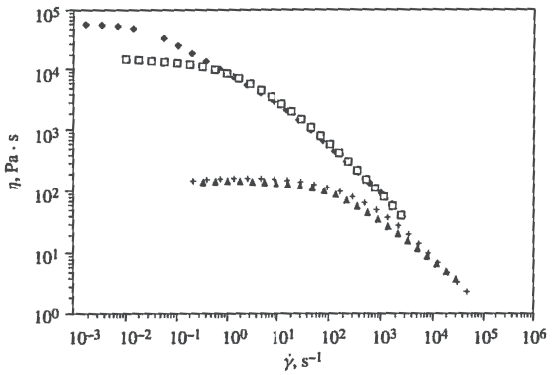

Figure 2.1 - Shear viscosity, η, as a function of shear rate $\dot{\gamma}$ for polydimethylsiloxanes with different molecular weights [Morrison, 2001].

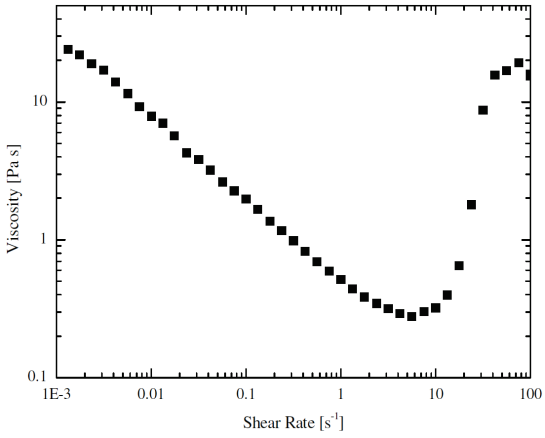

Figure 2.2 - Shear viscosity as a function of shear rate for a 55 % concentration of cornstarch in water suspension [White et al., 2009].

Here again n is a coefficient determining the slope of the exponential region, η_0 is the viscosity limit at low shear rates, η_∞ is the viscosity limit at high shear rates, a is a factor determining the width of the transition region and λ determines the shear rate, where the transition starts. Both models can model shear thinning and thickening. In the power law model shear thinning is simulated when $0 < n < 1$, while shear thickening is replicated when $n > 1$. For the Carreau-Yasuda model $0 < n < 1$, and shear thinning is simulated when $\eta_0 > \eta_\infty$ while for shear thickening $\eta_0 < \eta_\infty$. The two models are compared on Figure 2.3 and Figure 2.4 for shear thinning and thickening, respectively. The Carreau-Yasuda model has the advantage that there are more coefficients, that can be used to curve fit your experimental data.

2.3 Memory effects

The fluid models described in Section 2.2 only simulate viscous effects. That means that all the energy is dissipated, and all references to earlier configurations are lost. Many fluids also have elastic effects, where a part of the stress is dependent on earlier configurations. This causes effects like the Weissenberg effect, which is seen in Figure 2.5, and die swell, seen in Figure 2.6. The Weissenberg effect is observed when an elastic liquid is stirred. Intuitively one would assume that the centrifugal forces will move the fluid away from whisk, but it is observed that the fluid climbs the whisk instead; a good example from the kitchen is dough which climbs the mixer blades. The effect occurs because the fluid is stretched like a rubber band, hence squeezing the blades, and since the outer "rubber bands" displaces the inner ones, these climbs the blades. Die swell is observed when an elastic fluid exits from a die into open air. As the elastic stresses are "released" the liquid stream increases in diameter. A way to incorporate elastic stress is to sum Hooke's law of an elastic solid with the Newton's law of viscosity. Newton's law of viscosity was derived for a Couette flow, depicted on Figure 2.7, where the fluid domain is infinite in the x- and z-direction, the bottom of the fluid is stationary and the top has a velocity, V. The shear viscous stress is given from (2.6) and (2.7):

$$\tau_{yx.visc} = -\mu \frac{du}{dy} = -\mu \dot{\gamma}_{yx}(t), \tag{2.10}$$

where u is the x-component of the velocity vector. The elastic shear stress is given by Hooke's law for small displacements:

$$\tau_{yx.elas} = -G \frac{dD}{dy} = -G \gamma_{yx}(t_{ref}, t), \tag{2.11}$$

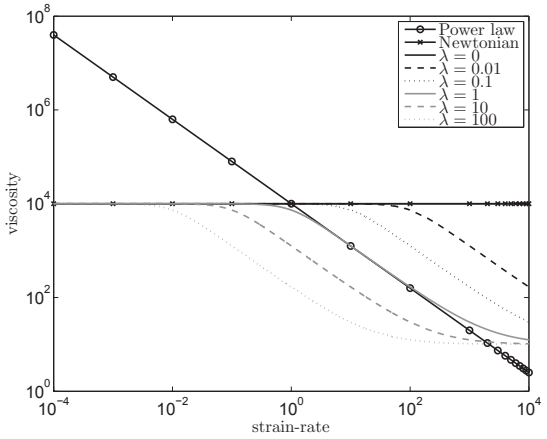

Figure 2.3 - Comparison of the power law model and the Carreau-Yasuda model for a shear thinning fluid. Power law model: $n = 0.1$, $m = 10000$. Carreau-Yasuda model: $n = 0.1$, $\eta_0 = 10000$ $\eta_\infty = 10$ and $a = 2$.

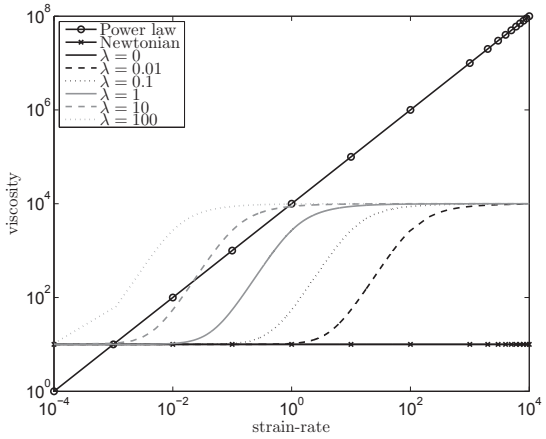

Figure 2.4 - Comparison of the power law model and the Carreau-Yasuda model for a shear thickening fluid. Power law model: $n = 2$, $m = 10000$. Carreau-Yasuda model: $n = 0.1$, $\eta_0 = 10$ $\eta_\infty = 10000$ and $a = 2$.

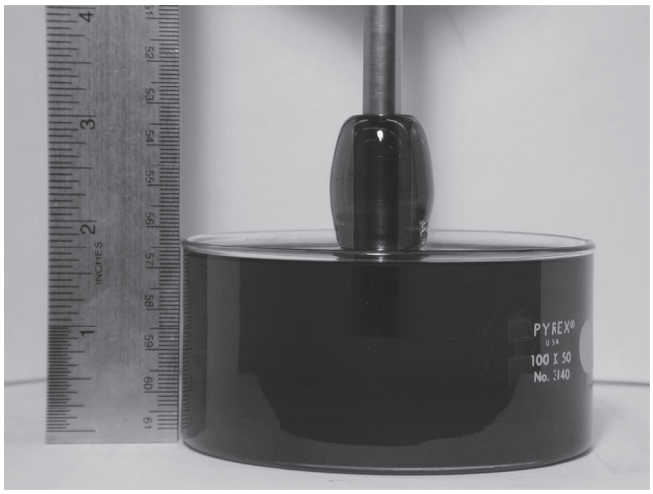

Figure 2.5 - The Weissenberg effect.

Figure 2.6 - The die swell effect.

where G is the shear stress modulus, D is the displacement in the x-direction and $\gamma_{yx}(t_{ref}, t)$ is the shear strain at time t with respect to the reference time t_{ref}. There is the following relationship between strain and strain-rate:

$$\gamma_{ij}(t_{ref}, t) = \int_{t_{ref}}^{t} \dot{\gamma}_{ij}(t')\, dt' \tag{2.12}$$

In 1867 James Clerk Maxwell proposed the following model:

$$\tau_{yx} + \frac{\mu}{G}\frac{\partial \tau_{yx}}{\partial t} = -\mu \dot{\gamma}_{yx}(t'), \tag{2.13}$$

and is known as the *Maxwell model*. As elasticity is based on a previous configuration, it is a time dependent quantity, and what this model does is that it mixes the two extreme cases, namely pure viscous and pure elastic behaviour. When $\frac{\partial \tau_{yx}}{\partial t} \to 0$, the model approaches Newton's law of viscosity in (2.10). On the other hand when $\frac{\partial \tau_{yx}}{\partial t} \gg \tau_{yx}$ then $\frac{\partial \tau_{yx}}{\partial t} = -G\dot{\gamma}_{yx} \Rightarrow \tau_{yx}(t) = -G \int_{t_{ref}}^{t} \dot{\gamma}_{yx}(t')\, dt' = -G\gamma_{yx}(t_{ref}, t)$ recovering Hooke's law, (2.11). The model can also be derived by considering a spring and dashpot in series, as seen in Figure 2.8. The spring force is given by:

$$f = -GD_{spring}, \tag{2.14}$$

where D_{spring} is the displacement of the spring. The force on the dashpot is given by:

$$f = -\mu \frac{dD_{dash}}{dt}, \tag{2.15}$$

where D_{dash} is the displacement of the dashpot. The total displacement is given by:

$$D_{total} = D_{spring} + D_{dash}. \tag{2.16}$$

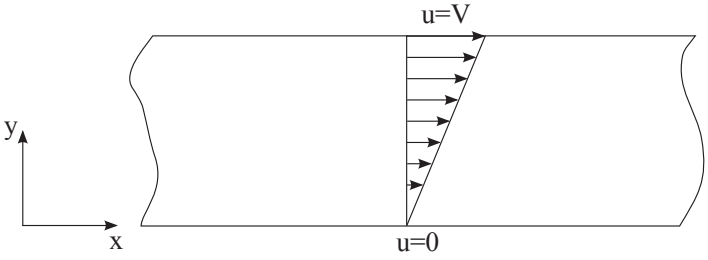

Figure 2.7 - The Couette flow.

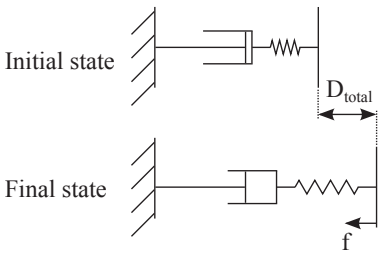

Figure 2.8 - Spring and dashpot in series.

Taking the time derivative and inserting (2.14) and (2.15) gives:

$$f + \frac{\mu}{G}\frac{df}{dt} = -\mu\frac{dD_{total}}{dt}, \tag{2.17}$$

which can be interpret as the Maxwell model. The *relaxation time* is defined as $\lambda = \frac{\mu}{G}$, and describes how long time elastic effects are present. After the relaxation time only viscous effects are present, and the earlier reference configuration has been "forgotten". It can be seen that when $G \ll \mu$ then $\lambda \to \infty$, and the system will always be dominated by elastic effects. When $G \gg \mu$ then $\lambda \to 0$, and the system reaches an inelastic state almost instantaneously. There are other spring dashpot systems, which lead to other equations, but all have the same objective, namely a part which conserves energy, and a part which dissipates energy. The Maxwell model can be generalised by replacing the scalar quantities of stress and strain-rates with tensor quantities:

$$\boldsymbol{\tau} + \lambda\frac{\partial \boldsymbol{\tau}}{\partial t} = -\eta_0\dot{\boldsymbol{\gamma}}. \tag{2.18}$$

There is also an integral version of this, where (2.18) is multiplied through by $\frac{e^{\frac{t}{\lambda}}}{\lambda}$, and integrated over all past times to the time of interest t. By requiring that the stress is finite at $t = -\infty$ the integral form of the Maxwell model is obtained:

$$\boldsymbol{\tau}(t) = -\int_{-\infty}^{t}\left[\frac{\eta_0}{\lambda}e^{\frac{-(t-t')}{\lambda}}\right]\dot{\boldsymbol{\gamma}}(t')\,dt', \tag{2.19}$$

where the term in the square brackets are the "variable forgetting function", while $\dot{\boldsymbol{\gamma}}(t')$ is the strain rate in the past times. It is seen that when $t \to \infty$, the exponential term approaches zero, meaning that the accumulated stress becomes smaller and smaller, hence the name "variable forgetting function". There is also a strain version given by:

$$\boldsymbol{\tau}(t) = \int_{-\infty}^{t}\left[\frac{\eta_0}{\lambda^2}e^{\frac{-(t-t')}{\lambda}}\right]\boldsymbol{\gamma}(t,t')\,dt', \tag{2.20}$$

2.4 Limitations to the Maxwell model

In 1950 James G. Oldroyd stated the mathematical requirements, that a rheological model must fulfill, [Oldroyd, 1950]. One of them is that the model shall be frame invariant, which means the flow predicted should be the same regardless of the coordinate frame of the system (Cartesian, polar, rotational etc.). The Maxwell model, (2.18), does not fulfill this, which can be shown in the so called *turntable experiment* developed in Bird et al. [1987]. Figure 2.9 shows a hypothetical test setup, where a Couette flow is produced by some devise, which is fixed on a turntable rotating with a constant angular velocity, Ω. By assuming that the fluid is described by the Maxwell model, and by calculating the strain rate and the stress one can derive the material properties, which should be independent of reference frame. The calculations are not performed here (see Bird et al. [1987] or Morrison [2001]), but it turns out that in the xyz-coordinate system, the material properties are dependent on Ω, which does not make sense at all. This makes the Maxwell model invalid as a constitutive model, but it has shown to be reliable in flows with small strain-rates.

The step where it went wrong was the transformation of the scalar equation (2.13) to the tensorial equation (2.18). The problem is that the infinitesimal strain tensor in the tensorial version does not transfer invariantly from a stationary reference frame to a rotating. So by applying the partial derivative to $\boldsymbol{\tau}$ the equation has become frame-variant equation.

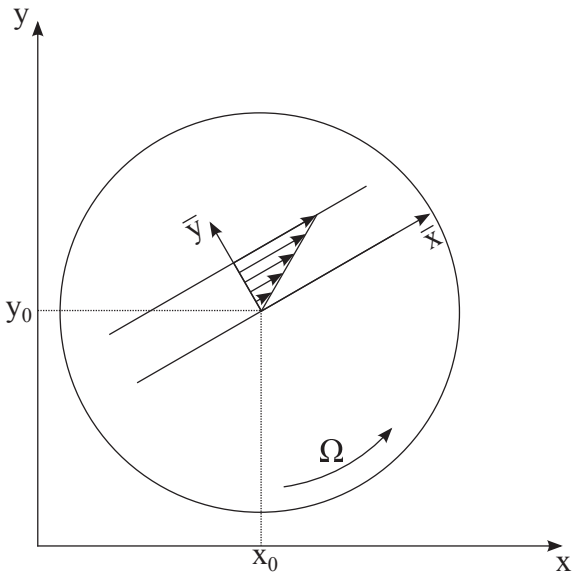

Figure 2.9 - Illustration of the turntable example

2.5 Large deformations

The flaw of the linear Maxwell model is that it uses the infinitesimal strain tensor, which does not separate rigid body rotation from the relative deformation, because only small strains are modelled properly. A way to remedy this is through the use of the polar decomposition theorem, which states that any tensor $\boldsymbol{A}$ for which an inverse $\boldsymbol{A}^{-1}$ exists has two unique decompositions:

$$\boldsymbol{A} = \boldsymbol{R} \cdot \boldsymbol{U} = \boldsymbol{V} \cdot \boldsymbol{R}, \tag{2.21}$$

where:

$$\boldsymbol{U} = (\boldsymbol{A}^T \cdot \boldsymbol{A})^{\frac{1}{2}} \tag{2.22}$$

$$\boldsymbol{V} = (\boldsymbol{A} \cdot \boldsymbol{A}^T)^{\frac{1}{2}} \tag{2.23}$$

$$\boldsymbol{R} = \frac{\boldsymbol{A}}{(\boldsymbol{A}^T \cdot \boldsymbol{A})^{\frac{1}{2}}} = \boldsymbol{A} \cdot \boldsymbol{U}^{-1}. \tag{2.24}$$

$\boldsymbol{R}$ is a pure rotation tensor; it changes the direction of an arbitrary vector, but it does not change its magnitude. This means that $\boldsymbol{U}$ and $\boldsymbol{V}$ contain all the stretch information of $\boldsymbol{A}$, and they are called right and left Cauchy-Green stretch tensors, respectively. The action of the right stretch tensor and rotation tensor is shown on Figure 2.10. The arbitrary vector $\boldsymbol{u}$ is transformed to $\boldsymbol{v}$ by the tensor $\boldsymbol{A}$. If this tensor is decomposed to a rotation part $\boldsymbol{R}$ and a stretch part $\boldsymbol{U}$, then $\boldsymbol{U}$ transforms $\boldsymbol{u}$ to $\boldsymbol{w}$, and $\boldsymbol{R}$ rotates $\boldsymbol{w}$ to produce $\boldsymbol{v}$. $\boldsymbol{w}$ and $\boldsymbol{v}$ have equal length and hence all stretching information lie in $\boldsymbol{U}$. The rotation which occurs from $\boldsymbol{u}$ to $\boldsymbol{w}$ is due to deformation. The choice of using the right or left stretch tensor is a matter of convenience. On Figure 2.11 the action of decomposition using both $\boldsymbol{U}$ and $\boldsymbol{V}$. Here the transformation is performed on the principal direction of $\boldsymbol{U}$, which are given by its eigenvectors, ξ_i. It is rotated to the principal direction of $\boldsymbol{V}$, given by its eigenvectors, ζ_i. Since $\boldsymbol{U}$ and $\boldsymbol{V}$ produce the stretch of an arbitrary vector they have the same eigenvalue, λ. If $\boldsymbol{U}$ is chosen it corresponds to follow the solid path on Figure 2.11, where first the stretch is produced by $\boldsymbol{U}$ and then the rotation is applied by $\boldsymbol{R}$. Using $\boldsymbol{V}$ is the same as to follow the dashed line on Figure 2.11 by first applying the rotation by $\boldsymbol{R}$ and then stretching it by the use of $\boldsymbol{V}$. Consider a body deforming over time shown on Figure 2.12. The relative distance between two arbitrary points are considered at two instances in time. The deformation that the nearby points experience between the time t and time t' is given by:

$$d\boldsymbol{r'} = d\boldsymbol{r} \frac{\partial \boldsymbol{r'}}{\partial \boldsymbol{r}}. \tag{2.25}$$

The tensor $\frac{\partial \boldsymbol{r'}}{\partial \boldsymbol{r}}$ is called the *deformation-gradient tensor*:

$$\boldsymbol{F}(t,t') = \frac{\partial \boldsymbol{r'}}{\partial \boldsymbol{r}}. \tag{2.26}$$

Alternatively:

$$d\boldsymbol{r} = d\boldsymbol{r'}\frac{\partial \boldsymbol{r}}{\partial \boldsymbol{r'}}, \tag{2.27}$$

where $\frac{\partial \boldsymbol{r}}{\partial \boldsymbol{r'}}$ is the *inverse deformation gradient tensor*:

$$\boldsymbol{F}^{-1}(t,t') = \frac{\partial \boldsymbol{r}}{\partial \boldsymbol{r'}}. \tag{2.28}$$

The deformations are independent of the rigid body linear displacement, but not the rigid body rotation, so polar decomposition is applied by using definitions in (2.22) and (2.23):

$$\boldsymbol{C} = \boldsymbol{F}\cdot\boldsymbol{F}^T \tag{2.29}$$

$$\boldsymbol{C}^{-1} = (\boldsymbol{F}^{-1})^T\cdot\boldsymbol{F}^{-1}, \tag{2.30}$$

where $\boldsymbol{C}$ is called the *Cauchy strain tensor* and $\boldsymbol{C}^{-1}$ is called the *Finger strain tensor*. Since the infinitesimal strain tensor used in the integral strain version of the linear Maxwell model, (2.20) describes the strain over all past times until the current time t, the infinitesimal strain tensor, $\boldsymbol{\gamma}$, is replaced with the Finger strain tensor, $\boldsymbol{C}^{-1}$:

$$\boldsymbol{\tau}(t) = -\int_{-\infty}^{t}\left[\frac{\eta_0}{\lambda^2}e^{\frac{-(t-t')}{\lambda}}\right]\boldsymbol{C}^{-1}(t,t')\,dt', \tag{2.31}$$

This is called the *Lodge equation*, and using this, the elasticity in a fluid is described correctly independent of the frame. The Lodge model is more familiar in its differential form, which is given by differentiating (2.31) with respect to time, applying integration by parts, using the product rule of differentiation and inserting (2.31) yields:

$$\frac{\boldsymbol{\tau}}{\lambda} + \left[\frac{d\boldsymbol{\tau}}{dt} - (\nabla\boldsymbol{u})^T\cdot\boldsymbol{\tau} - \boldsymbol{\tau}\cdot\nabla\boldsymbol{u}\right] = -\frac{\eta_0}{\lambda}\boldsymbol{I}, \tag{2.32}$$

where $\boldsymbol{u}$ is the velocity vector and $\boldsymbol{I}$ is the identity tensor. In general it is not possible to separate normal viscous stresses from the pressure (for Newtonian fluids its no problem as the normal viscous stress are zero in shear flows). $\boldsymbol{\tau}$ is therefore only known within an isotropic constant, so by defining a new stress tensor to be:

$$\boldsymbol{\varsigma} = \boldsymbol{\tau} + \frac{\eta_0}{\lambda}\boldsymbol{I}, \tag{2.33}$$

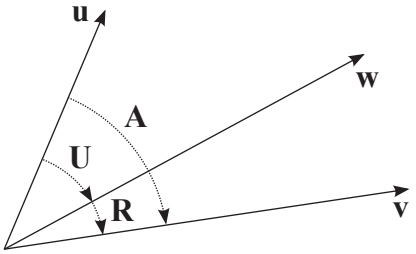

Figure 2.10 - Polar decomposition.

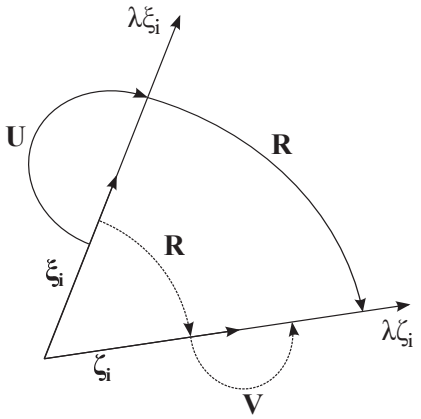

Figure 2.11 - Action of the different stretch tensors.

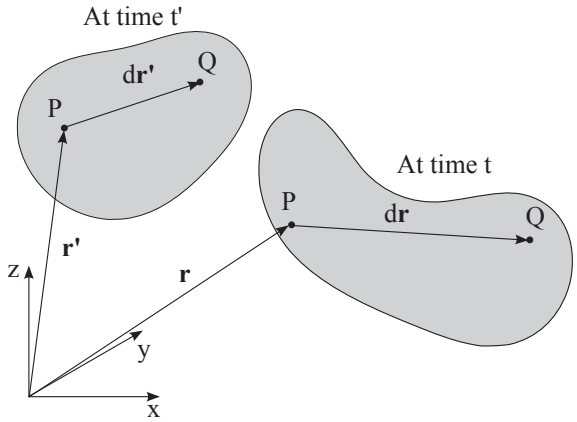

Figure 2.12 - Body deforming over time.

the following equation is achieved:

$$\boldsymbol{\tau} + \lambda \left[\frac{d\boldsymbol{\tau}}{dt} - (\nabla \boldsymbol{u})^T \cdot \boldsymbol{\tau} - \boldsymbol{\tau} \cdot \nabla \boldsymbol{u} \right] = \boldsymbol{\tau} + \lambda \overset{\nabla}{\boldsymbol{\tau}} = -\eta_0 \dot{\boldsymbol{\gamma}}. \tag{2.34}$$

Here the expression in the brackets is called the upper convected derivative of the stress tensor or the upper convected stress tensor, and it is denoted by $\overset{\nabla}{\boldsymbol{\tau}}$. Equation (2.34) is called the *upper convected Maxwell model*. Convected coordinates and derivatives can also be applied to derive (2.34). As the derivation is quite lengthy only the main idea is stated here. On Figure 2.13 a body is shown at different instances in time. The body has the $\hat{x}^1\hat{x}^2\hat{x}^3$ coordinate system attach to it, which deforms with the body. At time $t' = t$ the material grid coincides with the global stationary xyz coordinate system. At all times material points like, P, Q and S maintains their material coordinates, but the basis $\hat{\boldsymbol{e}}^1$, $\hat{\boldsymbol{e}}^2$ and $\hat{\boldsymbol{e}}^3$ change over time. A vector $\boldsymbol{r}$ can be expressed as:

$$\boldsymbol{r} = \hat{x}^1\hat{\boldsymbol{e}}^1 + \hat{x}^2\hat{\boldsymbol{e}}^2 + \hat{x}^3\hat{\boldsymbol{e}}^3, \tag{2.35}$$

and its differential is given by:

$$d\boldsymbol{r} = \frac{\partial \boldsymbol{r}}{\partial \hat{x}^1} d\hat{x}^1 + \frac{\partial \boldsymbol{r}}{\partial \hat{x}^2} d\hat{x}^2 + \frac{\partial \boldsymbol{r}}{\partial \hat{x}^3} d\hat{x}^3. \tag{2.36}$$

The basis vector for the convected coordinate system is given by:

$$g_{(i)} = \frac{\partial \boldsymbol{r}}{\partial \hat{x}^i} \tag{2.37}$$

Using these basis vectors to express the viscous stress tensor and relating it to the Cartesian coordinate system one arrives at:

$$\frac{d\hat{\boldsymbol{\tau}}}{dt} = \frac{d\boldsymbol{\tau}}{dt} - \left[\boldsymbol{\tau} \cdot \nabla \boldsymbol{u} + (\nabla \boldsymbol{u})^T \boldsymbol{\tau} \right]. \tag{2.38}$$

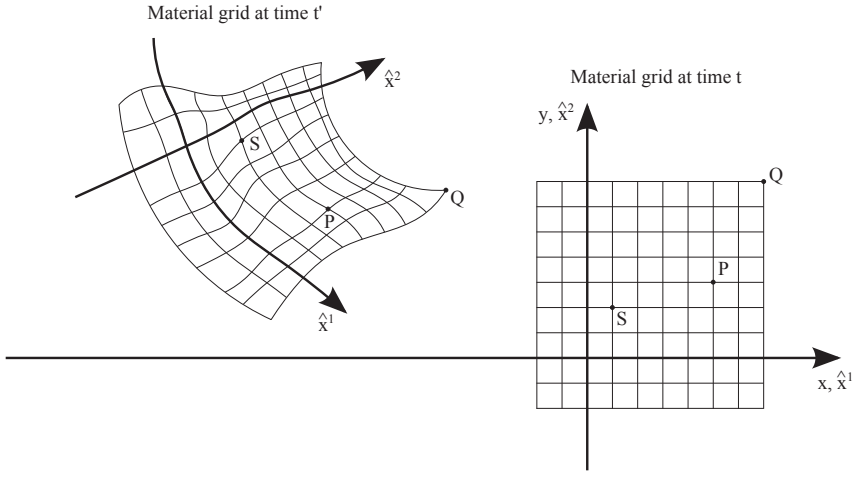

Figure 2.13 - Material grid described at different instances in time.

Which is the viscous stress in the $\hat{x}^1\hat{x}^2\hat{x}^3$ coordinate system differentiated with respect to time, and it is seen that it is the upper convected stress tensor of (2.34). Replacing $\frac{\partial \boldsymbol{\tau}}{\partial t}$ in (2.18) with (2.38) one arrives at (2.34), and it makes it frame independent. For a fully detailed derivation refer to Morrison [2001].

There are several other models which are extensions to the Maxwell model, and some of them will shortly be mentioned:

- **Upper convected Jeffreys or Oldroyd B model**

$$\boldsymbol{\tau} + \lambda_1 \overset{\nabla}{\boldsymbol{\tau}} = -\eta_0 \left(\dot{\boldsymbol{\gamma}} + \lambda_2 \overset{\nabla}{\dot{\boldsymbol{\gamma}}} \right) \tag{2.39}$$

  The Jeffreys model takes the strain rate at earlier times into account. The constant λ_2 is called the retardation time, and describes a time scale for the stress build up.
- **White-Metzner model**

$$\boldsymbol{\tau} + \frac{\eta(\dot{\gamma})}{G_0} \overset{\nabla}{\boldsymbol{\tau}} = -\eta(\dot{\gamma})\dot{\boldsymbol{\gamma}} \tag{2.40}$$

  The White-Metzner model takes shear thinning and thickening into account by replacing the viscosity with e.g. a power law model. G_0 is a constant modulus parameter.
- **Oldroyd 8-constant model**

$$\begin{aligned} \boldsymbol{\tau} + \lambda_1 \overset{\nabla}{\boldsymbol{\tau}} + \frac{1}{2}(\lambda_1 - \mu_1)(\dot{\boldsymbol{\gamma}} \cdot \boldsymbol{\tau} + \boldsymbol{\tau} \cdot \dot{\boldsymbol{\gamma}}) + \frac{1}{2}\mu_0(tr(\boldsymbol{\tau}))\dot{\boldsymbol{\gamma}} + \frac{1}{2}\nu_1(\tau : \dot{\boldsymbol{\gamma}})\boldsymbol{I} \\ = \eta_0 \left[\dot{\boldsymbol{\gamma}} + \lambda_2 \overset{\nabla}{\dot{\boldsymbol{\gamma}}} + (\lambda_2 - \mu_2)(\dot{\boldsymbol{\gamma}} \cdot \dot{\boldsymbol{\gamma}}) + \frac{1}{2}\nu_2(\dot{\boldsymbol{\gamma}} : \dot{\boldsymbol{\gamma}})\boldsymbol{I} \right] \end{aligned} \tag{2.41}$$

  The model was proposed by Oldroyd to include nonlinearities. By varying the constants λ_1, λ_2, μ_0, μ_1, μ_2, ν_1 and ν_2 produces various other constitutive models.
- **Giesekus model**

$$\boldsymbol{\tau} + \lambda \overset{\nabla}{\boldsymbol{\tau}} + \frac{\alpha\lambda}{\eta_0}\boldsymbol{\tau} \cdot \boldsymbol{\tau} = -\eta_0\dot{\boldsymbol{\gamma}} \tag{2.42}$$

  The Giesekus model incorporates a nonlinear stress term based on molecular arguments.

3 High Order Finite Element Theory

This chapter will describe some of the benefits of using a high order or spectral FEM (also known as Spectral Element Method (SEM)) compared to a traditional FEM. The FEM was mainly developed in the 1960s to address structural problems. Through the Principle of Virtual Work (PVW) the governing equations are put into variational form, where expansions of the unknowns (usually the displacements) allow the setup of an algebraic system of equations, which then can be solved. This is a very physical approach, where the equilibrium equations are multiplied with an arbitrary virtual displacement and the whole term is integrated over the domain of interest producing a virtual work. Through the use of the product rule of differentiation and Gauss' divergence theorem the final variational equation is produced. The contributions from the internal work, body forces and external forces are clearly identified giving an intuitive application [Cook et al., 2002].

The use of FEM in fluid dynamics was accelerated in the late 1970s. Instead of a virtual displacement, a virtual velocity is multiplied on the governing equations, and a formulation of the virtual power is achieved. Generally it can be said that one takes the inner product of the governing equations and some arbitrary test or weight function. This corresponds to projecting your equation to some vector space. Babuška [1973] and Brezzi [1974] addressed the instabilities arising when projecting velocity and pressure to incompatible vector spaces, formulating the *inf-sup*-condition, giving a theoretical tool of formulating stable FEM schemes for mixed problems.

Gottlieb and Orszag [1977] presented the theory, which is the backbone of the modern spectral methods, and there is quite a lot of literature on the subject, and especially Karniadakis and Sherwin [2005] and Rønquist [1988] are emphasised. Spectral methods showed superior convergence rates for smooth and well-behaved functions compared to traditional FEM.

3.1 The theory of SEM

Setting of in some linear Partial Differential Equation (PDE):

$$\mathcal{L}(u(\boldsymbol{x})) = f(\boldsymbol{x}), \tag{3.1}$$

where u is the unknown and f is a known function, which both can be dependent on the spatial coordinates symbolised by the spatial vector $\boldsymbol{x}$. Putting this in variational form by multiplying with a weight function (the virtual term), $v(\boldsymbol{x})$, and integrating over the domain, Ω:

$$\int_{\Omega} \left(\mathcal{L}(u(\boldsymbol{x})), v(\boldsymbol{x})\right) = \int_{\Omega} \left(f(\boldsymbol{x}), v(\boldsymbol{x})\right). \tag{3.2}$$

Depending on the linear operator, $\mathcal{L}$, the equation can be rewritten to a more applicable form. $u(\boldsymbol{x})$ and $v(\boldsymbol{x})$ can be represented as a series expansion:

$$u(\boldsymbol{x}) = \sum_{i=0}^{\infty} a_i \phi_i(\boldsymbol{x}) \tag{3.3a}$$

$$v(\boldsymbol{x}) = \sum_{i=0}^{\infty} b_i \psi_i(\boldsymbol{x}), \tag{3.3b}$$

where a_i and b_i are coefficients, and ϕ_i and ψ_i are basis functions. The approximations are introduced by truncating these to finite sums:

$$u(\boldsymbol{x}) \approx u_N(\boldsymbol{x}) = \sum_{i=0}^{N} a_i \phi_i(\boldsymbol{x}) \tag{3.4a}$$

$$v(\boldsymbol{x}) \approx v_N(\boldsymbol{x}) = \sum_{i=0}^{N} b_i \psi_i(\boldsymbol{x}), \tag{3.4b}$$

From this it is evident, that the higher truncation number, the better approximation, and hence already here it is revealed that low order FEM should be inferior to spectral methods, when it comes to approximating the exact function. It is also seen that since these series are smooth, non-smooth features are not approximated well using spectral methods. To remedy this the overall domain can be split into a number of subdomains capturing the non-smooth points at the interfaces, and then expand each subdomain with a high order polynomial. From (3.2) and (3.4b) it is clear that b_i are common factors, and since these in general are different from zero, they will be cancelled out. Therefore the unknowns solved for will be the coefficients, a_i. The schemes are varied by choosing different expansion polynomials, $\psi_i(\boldsymbol{x})$, where some of them are listed below:

- **The collocation method** is given by setting $\psi_i(\boldsymbol{x}) = \delta(\boldsymbol{x} - \boldsymbol{x}_j)$, where $\delta(\boldsymbol{x} - \boldsymbol{x}_j)$ is the Dirac delta function, which equals to one at the point $\boldsymbol{x}_j$ (called a collocation point) and zero everywhere else
- **The least squares method** minimises the $(\boldsymbol{R}, \boldsymbol{R})$, where $\boldsymbol{R} = f(\boldsymbol{x}) - \mathcal{L}(u(\boldsymbol{x}))$ is the residual, which for an exact solution should be zero. This is done by setting $\psi_i(\boldsymbol{x}) = \frac{\partial \boldsymbol{R}}{\partial a_i}$
- **The Galerkin method** sets the expansion polynomial for the test function to be equal to the expansion polynomial for the unknown, $\psi_i(\boldsymbol{x}) = \phi_i(\boldsymbol{x})$
- **The Petrov-Galerkin method** chooses any other expansion polynomial than the expansion polynomial for the unknown, $\psi_i(\boldsymbol{x}) \neq \phi_i(\boldsymbol{x})$

The choice of method comes down to preferences, but the most popular seems to be the collocation method and the Galerkin method, due to their simple implementation. The former has the nice feature, that the coefficient a_i equals the discrete value of the unknown, $u_N(\boldsymbol{x})$, at the collocation point, but the Galerkin method has a slight faster convergence [Gottlieb and Orszag, 1977]. The least squares method has the nice property that it circumvents the *inf-sup* condition and that it has a symmetric matrix for the convection-operator, which in other methods typical is anti-symmetric. This gives a great advantage, when it comes to solving the equation system.

As seen in (3.4a) and (3.4b) the approximation improves as $N \to \infty$, but not all expansion polynomials are appropriate. When multiplying with a test function, as in (3.4b), a projection to a vector space is actually performed, where each term in the multiplication of the two summations represents a dimension. If these orientations are non-orthogonal they will approach linear dependency to each other as the dimensions increase (when the degree of the polynomial increase). This will cause the system of equations to become ill-conditioned, yielding false solutions, or no solutions at all.

Polynomials are said to be orthogonal in the range $[a, b]$ if:

$$\int_a^b w(x)p_m(x)p_n(x)dx = \delta_{mn}c_n, \tag{3.5}$$

where $w(x)$ is a weighting function, δ_{mn} is the Kronecker delta, and c_n is a constant. If an orthogonal polynomial is used as a basis, then only polynomials of the same order will produce a non-zero term. There are numerous classes of polynomials with this property, and they are typically the solution to the Sturm-Liouville differential equation. Two of the most commonly used polynomials are the *Chebyshev*- and the *Legendre*-polynomials. Both are integrated over the interval $[-1, 1]$, but the Chebyshev polynomials have $w(x) = \frac{1}{\sqrt{1-x^2}}$ and $c_n = \begin{cases} \pi & \text{for n=0} \\ \frac{\pi}{2} & \text{otherwise} \end{cases}$, where the Legendre polynomials have $w(x) = 1$ and $c_n = \frac{2}{2n+1}$.

The following example originates from Karniadakis and Sherwin [2005]. A Galerkin approach is applied to discretise the following weak formulation:

$$(v_N, u_N) = (v_N, f), \tag{3.6}$$

which can be written in the following linear equation system:

$$\boldsymbol{Ma} = \boldsymbol{b}, \tag{3.7}$$

where the mass matrix is given by: $M_{pq} = (\phi_p, \phi_q)$, and the right hand side is given by: $b_p = (\phi_p, f)$. The solution is given by multiplying (3.7) with the inverse of $\boldsymbol{M}$. Three different expansion polynomials are compared on the interval $[-1, 1]$.

- **The moment expansion** simply increases the order of x in a monomial fashion, such that the set of order P contains all sets of lower order, $\mathcal{X}_{P-1} \subset \mathcal{X}_P$; so if $\mathcal{X}_2 = \{1, x, x^2\}$ then $\mathcal{X}_3 = \{1, x, x^2, x^3\} = \mathcal{X}_2 \bigcup \{x^3\}$. The mass matrix is given by:

$$M_{pq} = \int_{-1}^{1} x^p x^q dx = \begin{cases} \frac{2}{p+q+1} & \text{for p+q even} \\ 0 & \text{for p+q odd.} \end{cases} \tag{3.8}$$

- **The nodal expansion** is expanded by Lagrange polynomials, which consists of P polynomials of order $P - 1$, and hence are non-hierarchical ($\mathcal{X}_{P-1} \not\subset \mathcal{X}_P$). The basis function is given by $\phi_p(x_q) = \delta_{pq}$. This resembles the collocation method, but with the clear distinction that in the collocation method, the equations are solved exactly in the collocation points, while in the nodal expansion the coefficients represent an approximate solution. There is no explicit form of the mass matrix as it is obtained using numerical integration, but for equispaced nodes, which are common in FEM, it is a full matrix.
- **Expansion using Legendre polynomials** gives a simple expression for the mass matrix:

$$M_{pq} = \int_{-1}^{1} L_p(x)L_q(x)dx = \frac{2}{2p+1}\delta_{pq}, \tag{3.9}$$

  which as seen is a diagonal matrix, and hence is very easy to invert.

A measure of how ill-conditioned a matrix is, is the condition number, where the higher the number, the more ill-conditioned the matrix is. Figure 3.1 shows the impact of the different expansion polynomials on the condition number measured in the $L2$-norm, κ_2. The condition number for a real symmetric matrix in the $L2$-norm is the ratio between the maximum and minimum eigenvalue, so for the Legendre polynomial expansion with order P this is $\kappa_2 = \frac{2}{\frac{2}{2P+1}} = 2P + 1$, and hence only increases with a factor two. As the inverse mass matrix is

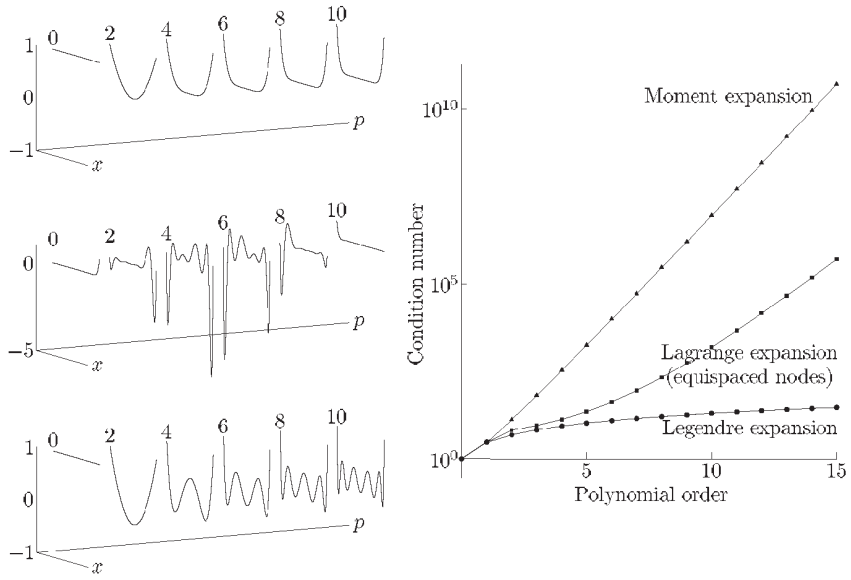

Figure 3.1 - To the left from top to bottom are the expansion polynomial at different orders for a moment, Lagrange and Legendre expansion, respectively. On the right the condition number is depicted as a function of the polynomial order. Taken from Karniadakis and Sherwin [2005]

full for both the moment and Lagrange polynomial expansions, the condition number will increase dramatically as the polynomial order is increased. This is confirmed on Figure 3.1, where $\kappa_2 \propto 10^P$ (however the Lagrange polynomials first starts this trend after $P \approx 5$). So by using orthogonal expansions it possible to use high order approximations, but still keeping the system solvable.

One more nice feature of using orthogonal polynomials is that there are clear relations between the orders, and to its derivatives as well. Recurrence relations can be derived for the different polynomials, and hence give an efficient computational implementation. The recurrence for the Legendre polynomials is:

$$\begin{aligned} nL_n(x) &= (2n-1)xL_{n-1}(x) - (n-1)L_{n-2}(x) \quad , \quad L_0(x) = 1 \quad , \quad L_1(x) = x \\ (1-x^2)L_n'(x) &= -nxL_n(x) + nL_{n-1}(x) = (n+1)xL_n(x) - (n+1)L_{n+1}(x). \end{aligned} \tag{3.10}$$

The recurrence for the Chebyshev polynomials is:

$$\begin{aligned} T_n(x) &= 2xT_{n-1}(x) - T_{n-2}(x) \quad , \quad T_0(x) = 1 \quad , \quad T_1(x) = x \\ (1-x^2)T_n'(x) &= nxT_n(x) - nT_{n+1}(x). \end{aligned} \tag{3.11}$$

3.2 Numerical example

To confirm the superior convergence rate of spectral methods for continuous and smooth functions a 1D test case is calculated using Legendre based expansion polynomials. The test case is:

$$\begin{aligned} \frac{d^2u}{dx^2} + 2\frac{du}{dx} + 10u &= f(x) \qquad \text{for} \qquad x = [-1, 1] \\ u(-1) + \left.\frac{du}{dx}\right|_{x=-1} &= 3 \\ u(1) + \left.\frac{du}{dx}\right|_{x=1} &= 1. \end{aligned} \tag{3.12}$$

For $f(x) = \sin(x)$ it has the solution depicted on Figure 3.2. Convergence rates are compared on Figure 3.3 in the infinity norm. It is clear that the p-refinement is superior to the h-refinement. Also the h-refinement has a linear convergence rate, while the p-refinement has an exponential

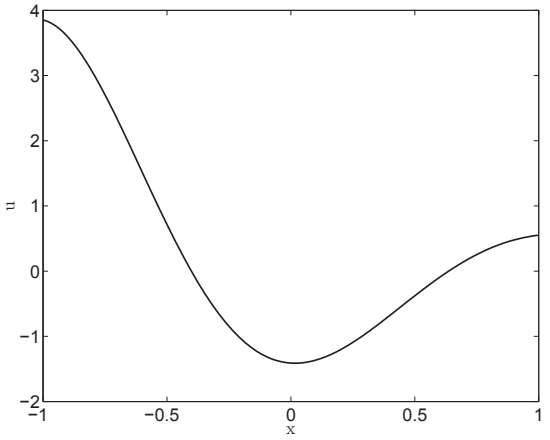

Figure 3.2 - Plot of test case in (3.12) with $f(x) = \sin(x)$

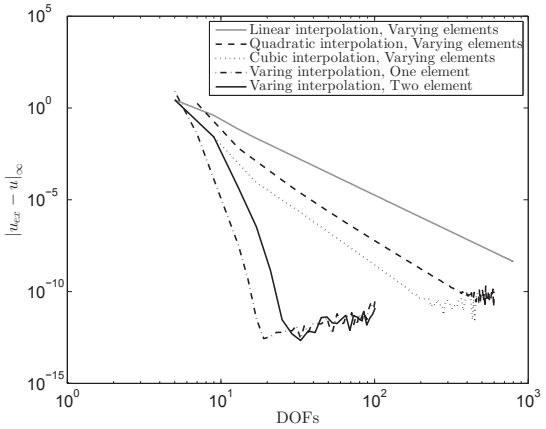

Figure 3.3 - Comparison of convergence rates for h- and p-refinement with $f(x) = \sin(x)$.

convergence rate. To show that spectral methods does not perform well for non-smooth functions $f(x)$ is set to the heaviside step function:

$$f(x) = H(x) = \begin{cases} 0 & \text{for x}<0 \\ \frac{1}{2} & \text{for x}=0 \\ 1 & \text{for x}>0 \end{cases} \tag{3.13}$$

The result is shown on Figure 3.4, and it is very similar to the smooth case in Figure 3.2, but the convergence rate for the case with varying interpolation and one element has really deteriorated as seen on Figure 3.5. It is also seen that a varying interpolation with 2 elements still have exponential convergence. This is due to the fact that the discontinuity of the forcing function is placed in the interface of the 2 elements.

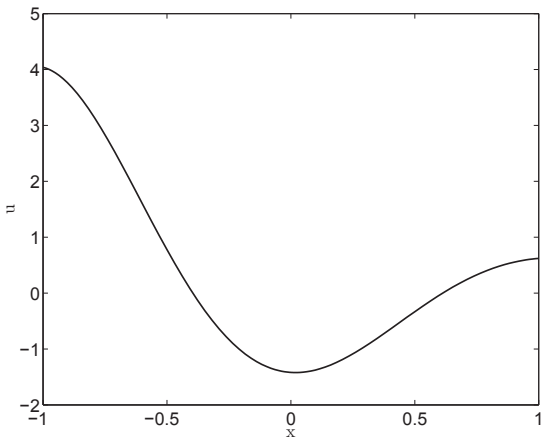

Figure 3.4 - Plot of test case in (3.12)

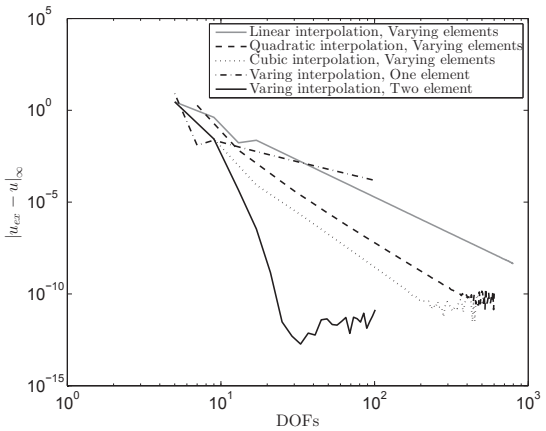

Figure 3.5 - Comparison of convergence rates for h- and p-refinement.

4 Mimetic Methods

This section describes the idea of mimetic or structure preserving methods, the general theory and ends with a draft paper, where the current suggestion to a structure preserving formulation is presented.

Equilibrium and balance equations are typically derived by observing an arbitrary finite domain, and then balancing both external and internal contributions of some physical quantity (e.g. forces, energy, mass etc.). Differential equations are obtained by applying theorems like the divergence theorem to relate the external contributions on surfaces to the volume of the domain, and then letting the size of the domain approach an infinitesimal value. The result is that all geometrical associations are lost, but equilibrium or balance equations should still be satisfied on any sub domain independently of its shape.

By structure preserving it is meant that the problem is discretised such that the balance equations are satisfied up to machine precision independently of the number of discrete values. All interpolations are located in the constitutive equations, which are empirical relations derived based on observations. In Palha [2013] and Kreeft [2013] mimetic methods are extensively explained, and in the latter reference the Stokes problem for a Newtonian fluid is discretised through a VVP formulation. The VVP formulation sets of in the Stokes equation:

$$-\operatorname{grad}(p) + \mu\, \Delta \boldsymbol{u} = \boldsymbol{f}, \tag{4.1}$$

and then the vorticity, $\boldsymbol{\omega} = \operatorname{curl}(\boldsymbol{u})$, is inserted giving:

$$\operatorname{grad}(p) + \mu \operatorname{curl}(\boldsymbol{\omega}) = \boldsymbol{f}, \tag{4.2}$$

The idea is to associate each physical quantity to a geometrical object, and then utilise the exact relations which exists between arbitrary geometrical objects their boundaries, namely the fundamental theorem of integrals:

$$\int_a^b \operatorname{grad}(f)\, ds = f(b) - f(a), \tag{4.3}$$

the Stokes theorem:

$$\iint_S \operatorname{curl}(\boldsymbol{F}) \cdot \boldsymbol{n}\, dS = \oint_{\partial S} \boldsymbol{F}\, ds, \tag{4.4}$$

and the divergence theorem:

$$\iiint_\Omega \operatorname{div}(\boldsymbol{F})\, d\Omega = \oiint_{\partial\Omega} \boldsymbol{F} \cdot \boldsymbol{n}\, dS. \tag{4.5}$$

Here f is a scalar, $\boldsymbol{F}$ is a vector, s is a line in space, S is a surface in space with the unit normal vector $\boldsymbol{n}$ and Ω is a volume in space. This can be summarised in the so-called discrete De Rham complex shown in Figure 4.1.

The orientation of a physical quantity must be taken into account. Orientation describes how a physical quantity is associated to a geometrical object. A physical quantity associated to a

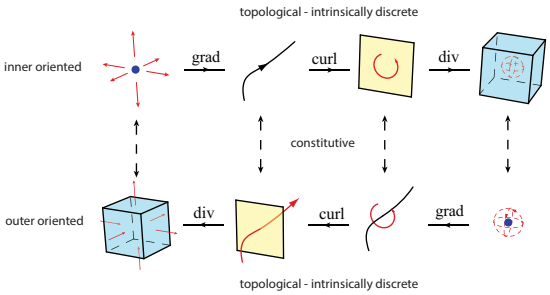

Figure 4.1 - Discrete De Rham complex.

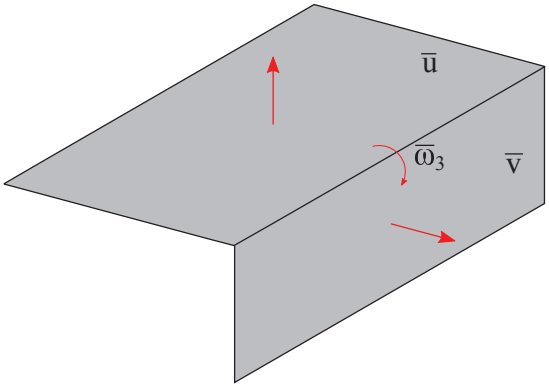

Figure 4.2 - Geometrical associations of the velocity and vorticity.

surface for instance can cross the surface (e.g. a momentum flux or a force), hence the name outer oriented, or it can rotate within the surface (e.g. a magnetic flux), hence the name inner oriented. The different orientations can be seen in Figure 4.1, where it is also observed that the constitutive equations are the link between the two orientations. The VVP formulation consists of three equations, namely $\boldsymbol{\omega} = \text{curl}(\boldsymbol{u})$, equation (4.2) and the incompressible continuity equation:

$$\text{div}(\boldsymbol{u}) = 0. \tag{4.6}$$

The procedure now is to associate the unknowns to geometrical objects, such that exact discrete relations can be established. Starting with the continuity equation then this describes the mass flux over the surfaces of a volume, but since the fluid is incompressible it becomes a velocity flux over a surface given by $\bar{\boldsymbol{u}} = \iint\limits_{\partial\Omega} \boldsymbol{u} \cdot \boldsymbol{n}\, dS$. So accordingly to (4.5) then by considering the velocity flux associated to surfaces as the unknown, the continuity equation applied to a volume can be described by summing all surface fluxes bounding the volume:

$$\iiint\limits_{\Omega} \text{div}(\boldsymbol{u})\, d\Omega = \sum_{i=1}^{N_S} \bar{u}_i, \tag{4.7}$$

where $\bar{u}_i$ is the velocity flux over a surface of the volume, and N_S is the number of surfaces bounding the volume. If a domain is decomposed into sub domains, then the continuity equation will always be satisfied in these sub domains by selecting the velocity flux associated to the boundaries of the sub domains as unknowns. The equation $\boldsymbol{\omega} = \text{curl}(\boldsymbol{u})$ can also be satisfied exact discretely. Figure 4.2 shows a cut out of a sub domain where two velocity flux components, $\bar{u}$ and $\bar{v}$ are shown. The vorticity is the rotation of the fluid, and since the two velocity fluxes are normal to their associated surfaces, the rotation describing this must be associated to the common edge of the two surfaces. So considering the vorticity integrated over the edges of the sub domains as unknowns, $\bar{\boldsymbol{\omega}} = \int\limits_{\partial S} \boldsymbol{\omega}\, ds$, then through the Stokes theorem, (4.4), the velocity flux on a surface will be given by summing the vorticity integrals from all its bounding edges:

$$\bar{\boldsymbol{u}} = \iint\limits_{\partial\Omega} \boldsymbol{u} \cdot \boldsymbol{n}\, dS = \iint\limits_{S} \text{curl}(\boldsymbol{\omega}) \cdot \boldsymbol{n}\, dS = \sum_{i=1}^{N_s} \bar{\omega}_i, \tag{4.8}$$

where $\bar{\omega}_i$ is the vorticity integrals around an edge of the surface, and N_s is the number of edges bounding the surface. It is not possible to apply any of the theorems to (4.2) in such a way that an exact discrete formulation is obtained, so this equation is not guaranteed to be satisfied in the discrete sense.

The choice of inserting the approximations in (4.2) is unfortunate because the momentum equations ought to be satisfied no matter size and shape of the sub domain. In this project the

flow is described by the Stokes equation with no forcing term:

$$-\operatorname{grad}(p) + \operatorname{div}(\boldsymbol{\tau}) = 0, \tag{4.9}$$

and the incompressible continuity equation, (4.6). The Stokes flow is a simplification of the general momentum equations, (2.1), where the convective term has been neglected. This is a good approximation for slow flowing high viscous fluids. Discretising (4.9), (4.6) and a constitutive equation, which here is chosen to be Newtons law of viscosity, (2.6), the balance equations are separated from constitutive equations. The problem is that $\boldsymbol{\tau}$ is a second order tensor, and the relations stated in the De Rham complex of Figure 4.1 only describes the relation between scalar values and vector values. By analysing the physical quantities, however, a discrete exact formulation can be derived. The momentum equations are derived by looking at the force balance on an arbitrary domain. For the Stokes equation the inertial term is neglected, the forces from $\boldsymbol{\tau}$ and p are external contributions acting on a surface, and the force term $\boldsymbol{f}$ in (4.2) is the body force in the domain (this is set to zero in this project). The viscous term should hence be described as the viscous stress integrated over the associated surface, which gives a force. This force can be regarded as a momentum flux of the surface. The pressure also produce a force normal to the surface, but since it is isotropic the size of the force will purely be dependent on the area of the surface, and this is unwanted because it will then be dependent on the size and shape of the sub domain. If instead the pressure is regarded a potential associated to a point this metric dependence is removed. This also corresponds with the use of the grad operator, which acts on scalars.

The conservation of mass is derived by looking at the mass balance of an arbitrary finite volume. By assuming incompressibility the only contribution is the mass flux over its boundaries, which also was the geometrical interpretation of the velocity in Kreeft [2013], but this does not comply well with the strain rate used in constitutive models. The strain rate is the rate of displacement between two arbitrary points of a deforming volume, so strain rate is geometrically associated to something which acts along a line. The velocity is therefore naturally associated to the points, which bound the strain rate line. So a more appropriate geometrical interpretation for the velocity is a vector associated to a point, which also complies with the divergence operator of the continuity equation, which naturally acts on vectors.

Figure 4.3 shows the location of the discrete unknowns for 2x2 grid in 2D for illustrative purposes. Notice that the velocity components are geometrically separated, and that they bound a sub element. The velocity fluxes over the surfaces of the sub element should be in perfect equilibrium.

The pressure and viscous forces bound sub cells which should have perfect force balance in the x-direction (marked with blue in Figure 4.3) and in the y-direction (marked with green). The location of the discrete values are described by a dual grid approach. A primal grid is built using Gauss Lobatto Legendre (GLL) points (marked with black lines in the upper left illustration of Figure 4.3), and a dual grid is constructed using Gauss Legendre (GL) points (marked with red lines in the upper left illustration of Figure 4.3). This is a normal approach in Palha [2013] and Kreeft [2013], where balance equations are described on individual grids, and then linked together through constitutive relations. Here a change in basis have been performed such that the physical quantities are located on both the primal and the dual grid. Notice though that the forces associated to the x-momentum are lying between the x-velocity components, and the forces associated to the y-momentum are lying between the y-velocity components. The link between these is the constitutive relations. This is done to be consistent with the physical behaviour, where stresses should be in the same space as the strain rates, which is the gradient of the velocity, and hence the stress should be one order lower than the velocity.

To obtain a square matrix system, the equations are put into variational form, and the weight function for continuity equation is chosen to be in the same space as the pressure, the weight

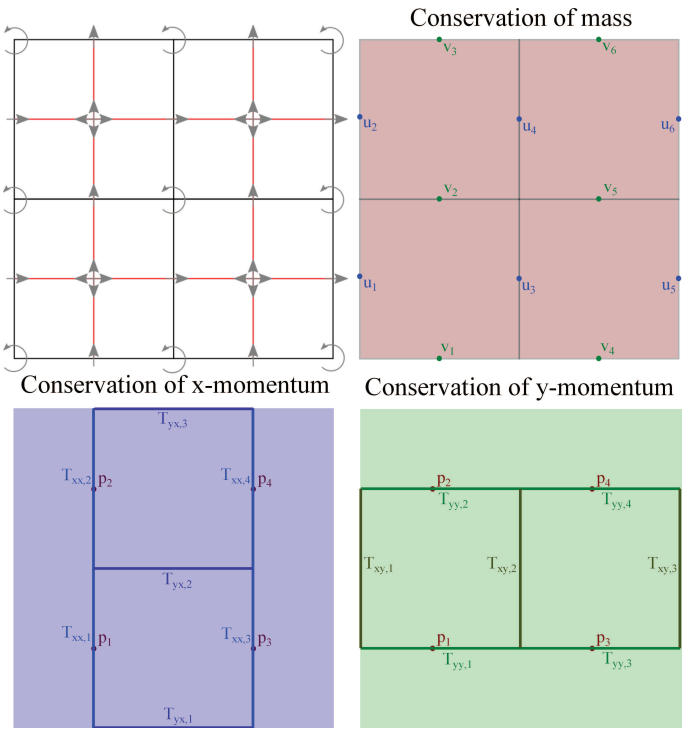

Figure 4.3 - Location of the discrete values of velocities, pressures and momentum fluxes.

function for the momentum equations is chosen to be in the same space as the velocity, and the weight function for the constitutive equation is chosen to be in the same space as the viscous forces. This is the traditional approach known from the Galerkin FEM, and perfect mass and momentum conservation are observed when applied to the lid driven cavity flow test case, but small spurious fluctuations in velocity are observed at the boundaries, which though diminish as the polynomial order is increased as seen on Figure 4.4. Considerable time has been invested to figure out what the root cause of these spurious oscillations is, and recently it was considered that compatibility between stress and velocity is not satisfied. Compatibility is shortly explained a requirement which are to be fulfilled to ensure that a strain-rate field has a unique velocity field associated to it. Remember the strain-rate tensor given in (2.7). It contains the gradient of the velocity field. So if the velocity field is given in a domain then a unique strain-rate field can be calculated. This is not the case for the opposite situation, where the strain-rate field is known. Say a reference velocity is known, and the velocity in an arbitrary point is desired, then this is accomplished by integrating. It is a fair requirement, that no matter which integration path that is chosen, then the result is the same. This is the compatibility requirement. This requirement is as mentioned always satisfied for the often used velocity-pressure formulation, where the stress is not solved for. There is a compatibility requirement in this formulation however, and that is the famous inf-sup condition formulated in Babuška [1973] and Brezzi [1974] saying that the pressure approximation space must be smaller than the velocity approximation space. In Maday and Patera [1989] it was shown that for spectral elements the pressure approximation space should be P_{N-2} if the velocity approximation space is P_N.

To achieve structure preservation it is required that the stresses are solved for, so a compatibility between stress and velocity is required. In Gerritsma and Phillips [1999] the compatibility requirements for the Velocity-Pressure-Stress (VPS) formulation was stated. The velocity-pressure requirement still follows Maday and Patera [1989], and the velocity-stress requirement is found to be that the approximation space of the stress should be *at least* the same size as the velocity space. This is however quite unfortunate because as seen above the stress space is smaller than the velocity space.

This is the current status of the formulation. The current idea to amend the issue of compatibility

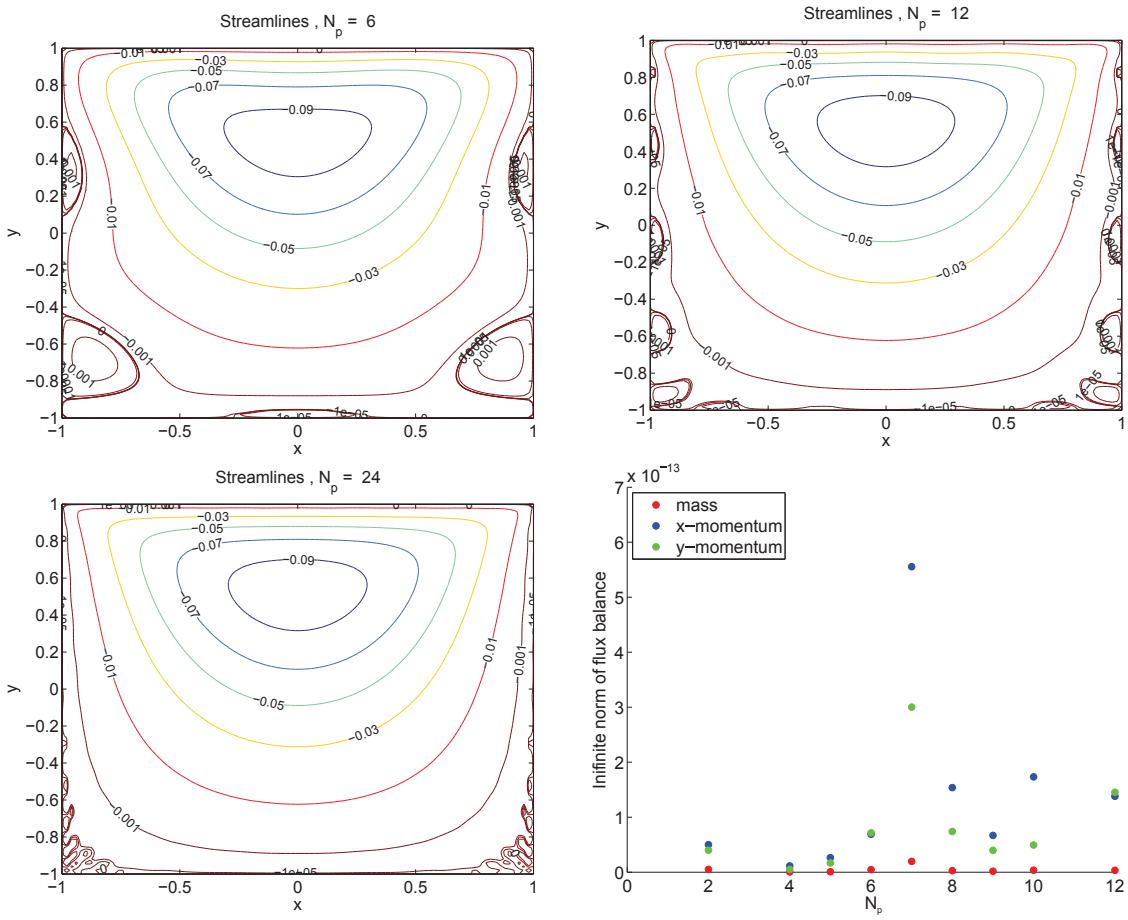

Figure 4.4 - Streamline plots with different polynomial order, and the last illustration shows the mass and momentum conservation of the mass and momentum cells, respectively, evaluated with the infinity norm.

is to choose a larger space for the stress, and then apply extra stress boundary conditions to ensure that the structure is preserved. A suggestion for such a formulation is outlined in the draft paper inserted below and will end this chapter. It is ongoing work and it reflects the status at the submission of the progress report. The paper is inserted with the format of this report.

STRUCTURE-PRESERVING FORMULATION OF STOKES FLOW

Kennet Olesen[1], Bo Gervang[2] and Marc Gerritsma[3]

Abstract

This paper describes conservation of mass and momentum in Stokes flow in terms. By a suitable choice of basis functions and an appropriate weak formulation mass and momentum are exactly conserved in the L^∞-norm. The method is applied to the lid-driven cavity problem.

Introduction

Conservation laws and constitutive equations play very distinct roles in physical models. Conservation laws express fundamental relations which need to be satisfied for all materials, whereas constitutive equations represent macroscopic relations of more fundamental processes at the microscopic level. Conservation laws are devoid of material parameters, while constitutive equations contain parameters which characterize the material under study. Earlier studies revealed that conservation laws can be exactly represented at the discrete level, while the numerical approximation occurs in the constitutive equations. In this paper we want to extend these ideas to vector-valued conservation laws, such as conservation of linear momentum in continuum mechanics.

In order to satisfy conservation of mass exactly at the discrete level, the velocity unknowns should be staggered similar to what has been done by Kopriva [1996], and what is common in staggered finite volume methods. As a result of this choice, the normal velocity components are readily available at the boundary, while the tangential velocity components are added using ghost points. This positioning of unknowns has consequences for the momentum equation. A weak formulation is presented in which the normal stress components are treated differently from the shear stress.

In Section 2 the weak formulation will be presented. In Section 3 the spectral basis functions and the treatment of boundary conditions will be introduced. Results of this spectral scheme will be given in Section 4 for Stokes flow in a the lid-driven cavity. Conclusions and future work are discussed in Section 5.

Weak formulation of Stokes formulation

Let Ω a bounded domain with Lipschitz boundary $\partial\Omega$, then the incompressible Stokes flow in vector notation is described by the momentum equation:

$$\operatorname{div}\sigma = -\operatorname{grad}(p) + \operatorname{div}\vec{\tau} = 0 \quad \text{in } \Omega\,, \tag{4.10}$$

together with conservation of mass for an incompressible medium:

$$\operatorname{div}\vec{u} = 0 \quad \text{in } \Omega\,, \tag{4.11}$$

and a suitably chosen constitutive model, which links the strain-rate to the stress. In this paper Newton's law of viscosity is chosen:

$$\vec{\tau} = 2\mu\vec{D}. \tag{4.12}$$

[1]Kennet Olesen
Aarhus University - Department of Engineering, Inge Lehmanns Gade 10, 8000 Aarhus, Denmark, e-mail: keol@eng.au.dk
[2]Bo Gervang
Aarhus University - Department of Engineering, Inge Lehmanns Gade 10, 8000 Aarhus, Denmark, e-mail: bge@ase.au.dk
[3]Marc Gerritsma
Delft University of Technology - Faculty of Aerospace Engineering, Kluyverweg 2, 2629 HS Delft, The Netherlands, e-mail: m.i.gerritsma@tudelft.nl

Here p is the pressure field, $\vec{u}$ is the velocity field, $\vec{\tau}$ is the second order viscous stress tensor, μ is the constant viscosity coefficient of the fluid, and $\vec{D}$ is the symmetric part of the strain-rate tensor

$$\vec{D} = \frac{1}{2}\left(\text{grad}^T\, \vec{u} + \text{grad}\, \vec{u}\right).$$

The model is supplemented by the boundary conditions

$$\vec{u} = 0 \quad \text{along } \partial\Omega\,.$$

Earlier work on mimetic spectral element methods for Stokes flow Hiemstra et al. [2014]; Kreeft and Gerritsma [2013] based on the vorticity-velocity-pressure (VVP) formulation, will not be used here. The VVP formulation is only applicable for constant viscosity coefficients and does not ensure conservation of linear momentum. This paper instead focuses on the velocity-pressure-stress formulation which can be used for non-constant viscosity coefficients and also guarantees force equilibrium. A similar approach was described in Toshniwal et al. [2014], but approach described in that paper was more akin to a spectral finite volume method.

In Gerritsma and Phillips [1999] a mixed velocity-pressure-stress formulation is given derived from a Lagrangian. In this paper a similar approach is applied with a slightly modified functional

$$\mathcal{L}(\vec{v}, q, \boldsymbol{\sigma}) = \frac{1}{4\mu}(\boldsymbol{\sigma} : \boldsymbol{\sigma}) - b(\boldsymbol{\sigma}, \vec{v}) + (q, \nabla \cdot \vec{v})\,, \tag{4.13}$$

where $q \in L^2(\Omega)$, $\vec{v} \in H(div;\Omega)$ and $\boldsymbol{\sigma} \in [H(div;\Omega)]_s^{2\times 2}$ which is the space of symmetric 2-tensors with square integrable coefficients and its divergence is square integrable.

Let the tensor $\boldsymbol{\sigma}$ begin by

$$\boldsymbol{\sigma} = \begin{pmatrix} \sigma_{\xi\xi} & \sigma \\ \sigma & \sigma_{\eta\eta} \end{pmatrix},$$

and the vector field $\vec{v} = (u, v)^T$ then the bilinear form $b(\boldsymbol{\sigma}, \vec{v}))$ in (4.13) is given by

$$b(\boldsymbol{\sigma}, \vec{v})) := \int_\Omega \left(-\frac{\partial \sigma_{\xi\xi}}{\partial \xi} u + \sigma \left(\frac{\partial u}{\partial \eta} + \frac{\partial v}{\partial \xi} \right) - \frac{\partial \sigma_{\eta\eta}}{\partial \eta} v \right) \mathrm{d}\Omega\,. \tag{4.14}$$

A stationary point $(\vec{u}, p, \tau)$ of the Lagrangian needs to satisfy the variational formulation

$$\begin{array}{lrll} & (\nabla \cdot \vec{v}, p) \quad -b(\boldsymbol{\tau}, \vec{v}) = 0 & \forall \vec{v} \in H(div;\Omega) \\ (\nabla \cdot \vec{u}, q) & = 0 & \forall q \in L^2(\Omega) \\ -b(\boldsymbol{\sigma}, \vec{u}) & +\frac{1}{2\mu}(\boldsymbol{\tau} : \boldsymbol{\sigma}) = 0 & \forall \boldsymbol{\sigma} \in [H(div;\Omega)]_s^{2\times 2} \end{array} \tag{4.15}$$

This system constitutes a symmetric, doubly constrained, mixed formulation, see Gerritsma and Phillips [1999]. For well-posedness the various function spaces need to satisfy appropriate inf-sup conditions.

In the discrete setting we select finite dimensional subspaces $Q \subset L^2(\Omega)$, $V \subset H(div;\Omega)$ and $T \subset [H(div;\Omega)]_s^{2\times 2}$ for which the variational statement reads: Find $(\vec{u}^h, p^h, \boldsymbol{\tau}^h) \in V \times Q \times T$ such that

$$\begin{array}{lrll} & (\nabla \cdot \vec{v^h}, p^h) \quad -b(\boldsymbol{\tau}^h, \vec{v}^h) = 0 & \forall \vec{v}^h \in V \\ (\nabla \cdot \vec{u}^h, q^h) & = 0 & \forall q^h \in Q \\ -b(\boldsymbol{\sigma}^h, \vec{u}^h) & +\frac{1}{2\mu}(\boldsymbol{\tau}^h : \boldsymbol{\sigma}^h) = 0 & \forall \boldsymbol{\sigma}^h \in T \end{array} \tag{4.16}$$

These discrete spaces have to satisfy compatibility conditions to ensure a unique solution. Let $\mathcal{Z}_V \subset V$ be the space of discrete vector fields, $\vec{v}^h$ which satisfy $\nabla \cdot \vec{v}^h = 0$, then $\mathcal{Z}_V^\perp \simeq Q$ leads to a locally mass conserving scheme. If $\mathcal{Z}_V^\perp$ is too large we only have approximate mass conservation, while if $\mathcal{Z}_V^\perp$ is too small spurious pressure oscillations will result. Finite dimensional spaces V and Q which satisfy $\mathcal{Z}_V^\perp \simeq Q$ have been studied in Hiemstra et al. [2014]; Kreeft and Gerritsma [2013]; Toshniwal et al. [2014] and will be used here.

Similarly, conditions between the finite dimensional velocity spaces V and T need to be imposed. Consider the space $\mathcal{Z}_T \subset V$ consisting of vector fields $\vec{v}^h$ for which the symmetric part of the velocity gradient vanishes, i.e.
$\mathcal{Z}_T = \{\vec{v}^h \in V \,|\, \boldsymbol{\nabla} v^h + \boldsymbol{\nabla}^T \vec{v}^h = 0\} \equiv \{\vec{v}^h \in V \,|\, b(\boldsymbol{\sigma}, \vec{v}^h) = 0, \;\; \forall \boldsymbol{\sigma} \in [H(div;\Omega)]_s^{2\times 2}\}$. Note that $\mathcal{Z}_T$ is the space of all solid body motions (translations and rotations). Compatibility now requires that $\mathcal{Z}_T^\perp \simeq T$. If $\mathcal{Z}_T^\perp$ is too large we satisfy conservation of momentum locally, but we have spurious velocity modes, while if $\mathcal{Z}_T^\perp$ is too small then we only approximate conservation of momentum. In case we prescribe both normal and tangential boundary conditions for the velocity – as we do in this paper –, we eliminate potential solid body motions, $\mathcal{Z}_T = \emptyset$.

Spectral element basis functions

In this paper we use a blend of basis functions. Let ξ_i, $i = 0, \ldots, N$ be the Gauss-Lobatto-Legendre (GLL) points of polynomial degree N and $\tilde{\xi}_i$, $i = 1, \ldots, N$ the Gauss-Legendre (GL) points. Note that $\xi_{i-1} < \tilde{\xi}_i < \xi_i$, for $i = 1, \ldots, N$. Furthermore, we introduce the extended Gauss-Legendre (EGL) points, $(\tilde{\xi}_0 = -1, \tilde{\xi}_i, \tilde{\xi}_{N+1} = 1)$, i.e. the Gauss-Legendre points plus the points -1 and 1. The Lagrange polynomials associated with the GLL points will be denoted by $h_i(\xi)$, the Lagrange polynomials associated with the GL points will be denoted by $\tilde{h}_i(\xi)$ and the Lagrange polynomials associated with the EGL points will be referred to as $\tilde{h}^e(\xi)$. From the Lagrange polynomials we can construct the polynomial edge functions, given by Gerritsma [2011]

$$e_i(\xi) = -\sum_{k=0}^{i-1} \mathrm{d}h_k(\xi) \;, \quad i = 1, \ldots, N \quad \text{and} \quad \tilde{e}_i = -\sum_{k=0}^{i-1} d\tilde{h}^e(\xi) \;, \quad i = 1, \ldots, N+1 \;.$$

$e_i(\xi)$ is a polynomial of degree $N-1$ and $\tilde{e}_i(\xi)$ is a polynomial of degree N. With these basis functions, we express the velocity field in a spectral element as

$$\vec{u}^h(\xi,\eta) = \sum_{i=0}^{N}\sum_{j=1}^{N} u_{i,j} h_i(\xi)\tilde{h}_j(\eta) + \sum_{i=1}^{N}\sum_{j=0}^{N} v_{i,j}\tilde{h}_i(\xi)h_j(\eta) \;. \tag{4.17}$$

Note that the ξ-component of the velocity is a polynomial of degree N in the ξ-direction and a polynomial of degree $N-1$ in the η-direction, $u \in \mathbb{P}^{N,N-1}$. Similarly, the η-component of the velocity field, $v \in \mathbb{P}^{N-1,N}$. It follows that $\operatorname{div} \vec{u} \in \mathbb{P}^{N-1,N-1}$ and therefore the pressure field will be expanded as

$$p^h(\xi,\eta) = \sum_{i=1}^{N}\sum_{j=1}^{N} p_{i,j} e_i(\xi) e_j(\eta) \;.$$

This combination of velocity and pressure expansion guarantees that $\mathcal{Z}_V^\perp \simeq Q$ and therefore we have exact mass conservation without spurious pressure modes. The only singular mode in the pressure field is the physical singular mode which states that the pressure is determined up to a constant. We can remove this mode by imposing

$$\int_\Omega p^h(\xi,\eta)\,\mathrm{d}\xi\mathrm{d}\eta = 0 \quad \Longleftrightarrow \quad \sum_{i=1}^{N}\sum_{j=1}^{N} p_{i,j} = 0 \;. \tag{4.18}$$

We expand extra-stress components as

$$\tau^h_{\xi\xi}(\xi,\eta) = \sum_{i=0}^{N+1}\sum_{j=1}^{N} \tau_{\xi\xi\,i,j}\tilde{h}^e_i(\xi)e_j(\eta) \;, \quad \tau^h_{\eta\eta}(\xi,\eta) = \sum_{i=1}^{N}\sum_{j=0}^{N+1} \tau_{\eta\eta\,i,j} e_i(\xi)\tilde{h}^e_j(\eta) \;,$$

and

$$\tau^h_{\xi\eta}(\xi,\eta) = \tau^h_{\eta\xi}(\xi,\eta) = \sum_{i=0}^{N}\sum_{j=0}^{N} \tau_{\xi\eta\,i,j} h_i(\xi)h_j(\eta) \;.$$

With these expansions we have that

$$\frac{\partial \tau^h_{\xi\xi}}{\partial \xi} = \sum_{i=1}^{N+1}\sum_{j=1}^{N}(\tau_{\xi\xi\, i,j} - \tau_{\xi\xi\, i-1,j})\tilde{e}_i(\xi)e_j(\eta) \in \mathbb{P}^{N,N-1} \ ,$$

and

$$\frac{\partial \tau^h_{\eta\eta}}{\partial \eta} = \sum_{i=1}^{N}\sum_{j=1}^{N+1}(\tau_{\eta\eta\, i,j} - \tau_{\eta\eta\, i,j-1})e_i(\xi)\tilde{e}_j(\eta) \in \mathbb{P}^{N-1,N} \ .$$

So, in terms of polynomial degree $\partial \tau^h_{\xi\xi}/\partial\xi$ is in the same space as the ξ-component of $\vec{u}^h$ and $\partial \tau_{\eta\eta}/\partial\eta$ is in the same polynomial space as the η-component of $\vec{u}^h$. However, since u needs to be zero on the left and right boundary, we need to constrain $\tau^h_{\xi\xi}$ by setting

$$\frac{\partial \tau^h_{\xi\xi}}{\partial \xi} = 0 \quad \text{for } \xi = \pm 1 \ .$$

Similarly we impose

$$\frac{\partial \tau^h_{\eta\eta}}{\partial \eta} = 0 \quad \text{for } \eta = \pm 1 \ .$$

With these additional constraints we ensure that $\partial \tau^h_{\xi\xi}/\partial\xi$ can be expresses in the discrete u-velocity space and vice versa, every u van be expressed in terms of the space of $\tau^h_{\xi\xi}$- derivatives. The same holds for $\partial \tau^h_{\xi\xi}/\partial\xi$ and v.

For the weak formulation of the shear stress we need to discretize the shear rates $\partial u/\partial\eta$ and $\partial v/\partial\xi$. These are given by:

$$\frac{\partial u}{\partial \eta} = \sum_{i=0}^{N}\sum_{j=0}^{N}(u_{i,j+1} - u_{i,j})h_i(\xi)\tilde{e}_j(\eta) \ , \tag{4.19}$$

$$\frac{\partial v}{\partial \xi} = \sum_{i=0}^{N}\sum_{j=0}^{N}(v_{i+1,j} - v_{i,j})\tilde{e}_i(\xi)h_j(\eta) \ , \tag{4.20}$$

Note that in (4.19) and (4.20) we introduced expansion coefficients which were not in the velocity expansion (4.17). These additional coefficients are used to insert the prescribed tangential velocity components along the boundary. So whenever in (4.19) we refer to $u_{i,0}$ or $u_{i,N+1}$ we replace it by the local tangential velocity and whenever we refer to $v_{0,j}$ and $v_{N+1,j}$ we replace these values by the prescribed tangential velocity at the left and right boundary, respectively.

Note that $\partial u/\partial\eta$ and $\partial v/\partial\xi$ are in the same polynomial space as the shear stress representation.

5 Conclusion

The content of this progress report reflects the current status of this PhD project. The majority of the time so far has been utilised to learn and understand the theory of rheology, high order methods and the mimetic method, as well as completing the required 30 ECTS points of courses. A structure preserving formulation of the Stokes problem has been suggested, which ought to preserve mass and momentum for arbitrary constitutive models.

Only selected theory of rheology has been presented in this report, and no numerical application has been given. This will be a substantial part of the future work.

It has been shown that the high order FEM obtains convergence rates, which is superior to low order methods. Non-smooth functions are not captured well by high order methods unless the non-smooth point is located at the interface between elements, in which case the convergence rate is unchanged. Since the rheological models described in this progress report in general are smooth, it is assessed that high order methods are applicable.

Considerable time have been spend to understand the essence of mimetic method, where Palha [2013] and Kreeft [2013] has been considerable inspirations as well as guidance from Marc Gerritsma. The topic extensively relies on differential geometry, which deliberately has been omitted in this report due to readability.

A formulation has been derived which preserves mass and momentum to machine precision independent of the resolution of the domain decomposition. This has been shown on the lid driven cavity test case. Spurious velocity oscillations are observed though, which have been traced to the non-satisfied compatibility condition between velocity and stress. This can be amended by choosing appropriate approximation spaces for the stress. Unfortunately if the stress space is too small compared to the velocity, spurious oscillations will be present, but if it becomes too large on the other hand, structure preservation is lost. Finding a formulation which satisfies these two requirements is currently ongoing work.

6 Future Work

This section is dedicated to describing how the remaining time of the PhD project will be utilised. It is divided in three sections, namely a theoretical part, an experimental part and an application part. The order of these sections corresponds to the order at which they will be executed in the project.

6.1 Theoretical

The general ideas and theory of the mimetic method are established, but a compatible formulation is still not found. Only the Newtonian fluid constitutive model has been considered, so more advanced models like the upper convected Maxwell model described in Section 2.5 is to be implemented. If the theory holds then mass and momentum should still be conserved to machine precision. The more advanced constitutive models will be challenging to discretise, because it is no longer possible to obtain explicit expressions for the stresses, and the non-linear expressions require iterative methods.

The current code is implemented in MATLAB using *for-loops*, which is very ineffective. The code is to be optimised through vectorisation and applying build-in operators. To really optimise the code for applications in 3D, the code should be written in C or C++. Resources like the *Fenics project*[1] could be applied.

6.2 Application

The mimetic method are to be compared with traditional high order methods and FVM, which is very common in commercial codes, due to its robustness. Various test cases are to be compared on convergence rates, efficiency and the ability to reproduce the correct flow pattern. Open source codes like *Nektar++*[2] for the high order methods and *Openfoam*[3] for the FVM are to be utilised.

6.3 Experimental

GEA Liquid Processing[4] in Skanderborg Denmark produces solutions for treatment and production of different liquids. They are currently developing their CFD capabilities, and have endorsed their support to experimental work on some of their products. One of their products is a high shear mixer, which mixes immiscible liquids like oil and water by applying high shear forces. The principle is shown on Figure 6.1. It resembles a centrifugal pump, but it has small holes in the casing. The immiscible liquids are lead into the impeller where they are mixed and then forced through the small holes. This introduces high shear forces, and a consistent liquid is produced. The resulting liquid is often high viscous, and have non-Newtonian properties. It could be interesting to determine these properties, and see if the flow trends could be reproduced in a simulation by applying an appropriate constitutive model.

[1] `http://fenicsproject.org`
[2] `http://www.nektar.info`
[3] `http://www.openfoam.com/`
[4] `http://www.gea-liquid.dk`

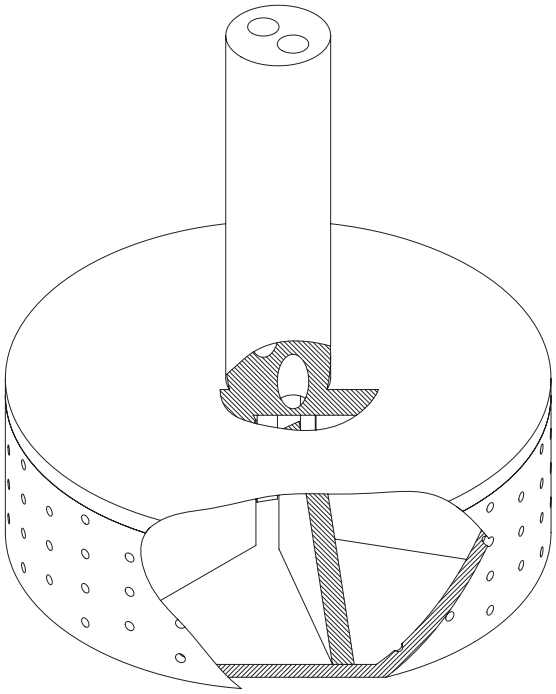

Figure 6.1 - High shear mixer consisting of an impeller rotating inside a casing with small holes.

Bibliography

Babuška, Ivo M. The finite element method with lagrangian multipliers. *Numer. Math*, 20:179, 1973.

Bird, R. Byron; Armstrong, Robert C., and Hassager, Ole. *Dynamics of Polymeric Liquids - Volume 1 Fluid Mechanics*. Number ISBN: 978-0-471-80245-7 in 2nd Edition. John Wiley and Sons, Inc., 1987.

Brezzi, Franco. On the existence, uniqueness and approximation of saddle-point problems arising from lagrangian multipliers. *RAIRO*, 8:129, 1974.

Cook, Robert D.; Malkus, David S.; Plesha, Michael E., and Witt, Robert J. *Concepts and Applications of Finite Element Analysis*. Number ISBN: 978-0-471-35605-9 in 4th Edition. John Wiley and Sons, Inc., 2002.

Gerritsma, Marc. Edge functions for spectral element methods. *Spectral and high order methods for partial differential equations - Lecture notes in computational science and engineering*, 76: 199–207, 2011.

Gerritsma, Marc and Phillips, Timothy N. Compatible spectral approximations for the velocity-pressure-stress formulation of the stokes problem. *SIAM*, 20-4:1530–1550, 1999.

Gottlieb, David and Orszag, Steven. *Numerical Analysis of Spectral Methods: Theory and Applications*. SIAM-CMBS, 1977.

Hiemstra, Rene; Toshniwal, Deepesh; Huijsmans, René, and Gerritsma, Marc. High order geometric methods with exact conservation properties. *Journal of Computational Physics*, 257: 1444–1471, 2014.

Karniadakis, George Em and Sherwin, Spencer J. *Spectral/hp Element Methods for CFD*. Number ISBN: 0-19-852869-8 in 2nd Edition. Oxford University Press, 2005.

Kopriva, David A. A conservative staggered-grid chebyshev multidomain method for compressible flows. *Journal of Computational Physics*, 125-1:244–261, 1996.

Kreeft, Jasper and Gerritsma, Marc. Mixed mimetic spectral element method for stokes flow: A pointwise divergence-free solution. *Journal of Computational Physics*, 240:284–309, 2013.

Kreeft, Jasper Jonas. *The Mimetic Spectral Element Method: A discretization of Geometry and Physics*. PhD-thesis from TU Delft, 2013.

Maday, Yvon and Patera, Anthony T. Spectral element methods for the incompressible navier-stokes equations. *State-of-the-art surveys on computational mechanics (A90-47176 21-64), ASME*, pages 71–143, 1989.

Morrison, Faith A. *Understanding Rheology*. Number ISBN: 978-0-19-514166-5 in 1st Edition. Oxford University Press, 2001.

Oldroyd, James G. On the formulation of rheological equations of state. *Proceedings of the Royal Society A*, 200:523–541, 1950.

Palha, Artur. *High order mimetic discretization: Development and application to Laplace and advection problems in arbitrary quadrilaterals.* PhD-thesis from TU Delft, 2013.

Rønquist, Einar Malvin. *Optimal Spectral Element Methods for the Unsteady Three-Dimensional Incompressible Navier-Stokes Equations.* PhD-thesis from Massachusetts Institute of Technology, 1988.

Toshniwal, Deepesh; Huijsmans, René, and Gerritsma, Marc. A geometric approach towards momentum conservation. *Lecture Notes in Computational SCience and Engineering*, 95: 393–402, 2014.

White, Erica E. Bischoff; Chellamuthu, Manoj, and Rothstein, Jonathan P. Extensional rheology of a shear-thickening cornstarch and water suspension. *Rheol Acta*, 49:119–129, 2009.

Glossary

Notation	Description
CFD	Computational Fluid Dynamics.
FDM	Finite Difference Method.
FEM	Finite Element Method.
FVM	Finite Volume Method.
GL	Gauss Legendre.
GLL	Gauss Lobatto Legendre.
PDE	Partial Differential Equation.
PVW	Principle of Virtual Work.
SEM	Spectral Element Method.
VVP	Vorticity-Velocity-Pressure.

Olesen, Kennet. Structure preserving formulation of high viscous fluid flows, 2014

Department of Engineering
Aarhus University
Inge Lehmanns Gade 10
8000 Aarhus
Denmark